

# Quantum spin transistors in superconducting circuits

Niels Jakob S e Loft,<sup>1,\*</sup> Lasse Bj rn Kristensen,<sup>1</sup> Christian Kraglund Andersen,<sup>1,2</sup> and Nikolaj T. Zinner<sup>1,3</sup>

<sup>1</sup>*Department of Physics and Astronomy, Aarhus University, DK-8000 Aarhus C, Denmark*

<sup>2</sup>*Department of Physics, ETH Zurich, CH-8093 Zurich, Switzerland*

<sup>3</sup>*Aarhus Institute of Advanced Study, Aarhus University, DK-8000 Aarhus C, Denmark*

(Dated: December 3, 2024)

Transistors play a vital role in classical computers, and their quantum mechanical counterparts could potentially be as important in quantum computers. Where a classical transistor is operated as a switch that either blocks or allows an electric current, the quantum transistor should operate on quantum information. In terms of a spin model the in-going quantum information is an arbitrary qubit state (spin-1/2 state). In this paper, we derive a model of four qubits with Heisenberg interactions that works as a quantum spin transistor, i.e. a system with perfect state transfer or perfect blockade depending on the state of two gate qubits. We propose a realistic implementation of the model using state-of-the-art superconducting circuits. Finally, we demonstrate that our proposal operates with high-fidelity under realistic decoherence, and without fine-tuning of any of the parameters.

## I. INTRODUCTION

When you look inside your personal computer, you will find integrated circuits filled with billions of miniscule transistors. Each transistor has a very simple job: it is a switch for opening or closing an electronic gate. Despite the limited functionality of each transistor, they achieve great things together, such as running your entire computer system. This approach to computing – connecting many simple devices into larger powerful structures – is called modular computing.

Modular computing allows for highly scalable and computationally capable classical computers. The same strategy can be employed in the quantum case [1], where various hybrid technologies [2, 3] such as cold atoms and photons [4, 5], superconducting circuits [6, 7] and optomechanical systems [8] have been proposed. Essentially, modular computing requires few-qubit modules that may readily enter into a larger network. Depending on the structure and operation of the network, one can achieve conditional dynamics [9], and ultimately build quantum computers [10], quantum simulators [11, 12], or quantum neural networks [13–15] for quantum machine learning [16–19].

Inspired by the crucial role the transistor plays in classical computers, we turn our attention towards its quantum analogue. Thought of as a module in a larger network [20], the quantum transistor is a link in a quantum information channel, and works as a switch for quantum state transfer. Implementations of such a gate has been studied as the atomtronic transistor in ultra-cold atoms [21–25], spintronic transistors [26–29], and photonic transistors based on light-matter interactions [30–34]. However, the usefulness of a quantum transistor is all the more clear when implemented with technologies that also allow for long-lived general-purpose qubits.

As the quantum transistor must enter as a component of a larger network, it must be capable of being mass-produced as a standard off-the-shelf unit. Thus, we propose in the work a design using superconducting circuits as these show great potential for producing commercial chips for quantum computing [6, 18, 35–38]. Specifically we show that an implementation using four interacting transmon qubits [39] is capable of realizing a high-quality quantum transistor. However, the transmon qubits can readily be exchanged for other types of qubits such as Xmon qubits[40], flux qubits[41–43], fluxonium qubits[44], phase qubits[45, 46], C-shunted flux qubits[47], and potentially other types of superconducting qubits. In Figure 1 we show a sketch of our proposed circuit and the resulting spin model of four interacting spins (qubits).

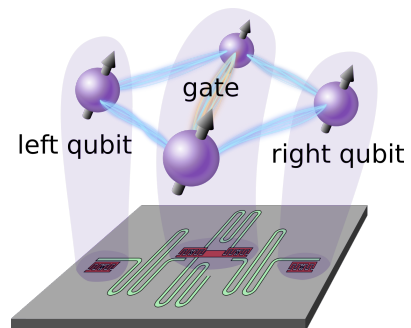


FIG. 1. Sketch of a superconducting circuit of four transmon qubits (red) coupled via resonators (green). Hovering above the circuit is the effective model of four spins/qubits (purple) interacting via Heisenberg XX couplings (blue) or Heisenberg XXZ couplings (blue and orange). Operated as a transistor, the two middle qubits comprise the gate, which is coupled to a left and a right qubit.

The four qubits in our implementation comprise of two gate qubits in the center connected to a left and a right qubit. Considered as a module in a larger network, the left and right qubits may connect the transistor to other parts of the network. In that respect, the transistor acts as a traffic junction in a road for quantum information, as

\* Present address: Research Laboratory of Electronics, Massachusetts Institute of Technology

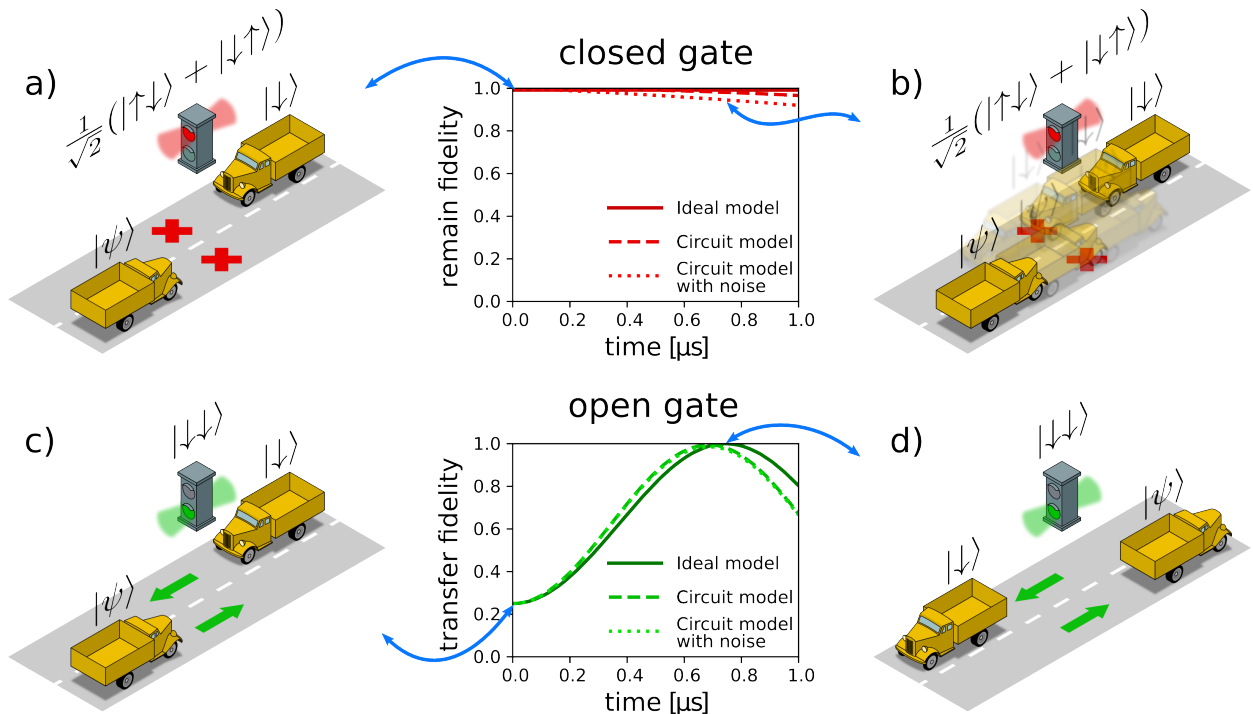


FIG. 2. Illustration of the transistor’s two functions with the gate as a traffic light, and the left and right qubit states loaded onto trucks. The graphs show simulation results for an ideal model (solid lines), our proposed circuit model with realistic parameters (dashed lines) and circuit model with realistic decoherence noise included (dotted lines) with  $|\psi\rangle = (|\uparrow\rangle + |\downarrow\rangle)/\sqrt{2}$ . The cartoons a)-d) illustrate the situations at various points on the graphs. **Closed gate:** The upper graph show the fidelity for remaining in the initial four-qubit state as a function of time. Ideally, the initial truck configuration a) will never change, i.e. a constant remain fidelity. However, in a realistic scenario, due to cross-talk couplings and noise, a small probability of running the red light emerges, indicated as ghostly trucks crossing the junction in b). **Open gate:** The lower graph show the state transfer fidelity as a function of time. The trucks initially on each side of the junction in c) will ideally cross the junction and transfer their load of quantum states to the opposite side, as seen in d). This state transfer happens with almost unit state fidelity also in the realistic scenario with noise.

depicted in Figure 2. Initially, an arbitrary qubit state  $|\psi\rangle$  is loaded onto the left truck, and a down-state  $|\downarrow\rangle$  is loaded onto the right truck. The two gate qubits constitute a traffic light, which may be red (closed gate) or green (open gate), depending on the their two-qubit state. For a perfect transistor with law-abiding truck drivers, the trucks would never run a red light, and would always cross with unit fidelity for a green light, thereby ensuring perfect blockade or transfer of the left and right qubit states. Thus the mechanism behind our transistor is blocking and allowing quantum state transfer. Typically this type of dynamics is studied in closed quantum systems[48–53] where the dynamics is symmetrical, but directional state transfer has also been studied recently [54, 55], which is interesting from a network point of view.

The first main result of this paper is providing a theoretical model for a four-qubit transistor. A significant finding is that our model does not require fine-tuning of the parameters in order to operate as a near-perfect transistor. We assess the performance of the transistor by the state-fidelity of the blocked or transferred state, shown as the solid lines on the plots on Figure 2. When the gate is closed, the fidelity to remain in the initial

(four-qubit) state is constant unity: The red light is on forever, and the trucks never move. On the other hand, when the gate is open, the state transfer fidelity grows smoothly to unity: The green light is on, and after some time the two trucks have crossed the junction. The initial state is here set as  $|\psi\rangle = (|\uparrow\rangle + |\downarrow\rangle)/\sqrt{2}$  to demonstrate the transistor’s capabilities to work with superposition states.

Our second main result is proposing a physical realizable model in superconducting circuits. This result includes realizing – for the first time to our knowledge – a direct fully-tuneable Heisenberg XXZ coupling between two superconducting qubits. In addition to the desired model, the superconducting circuit also give rise to a small ‘cross-talk’ coupling between the left and right qubits which prones the closed gate to leak slightly over time. However, this problematic coupling can be suppressed. Simulation results are shown as dashed lines on Figure 2.

Finally, we add experimentally realistic dephasing to the model and simulate its behavior. The dynamics of the noisy system is seen as the dotted lines on Figure 2. The most notable difference from the noiseless circuit

simulations (dashed lines) are a faster leakage of the closed transistor. However, within the relevant time-scale of operation, i.e. the transfer time, the state fidelity for the ideal state stays above 0.95, demonstrating very robust functionality.

This paper is organized as follows: In Section II, beginning from a very general four-qubit Heisenberg model, we determine which conditions the interaction constants must fulfill in order to realize a transistor and thus end up with an ideal transistor model. Using the idealized model as a stepping stone, we introduce in Section III a slightly more sophisticated model that can realistically be implemented with superconducting qubits. Section IV provides simulations of the proposed implementation.

Unless stated otherwise, we use units where  $\hbar = 2e = 1$ .

## II. A SIMPLE FOUR-QUBIT TRANSISTOR

The concept of the quantum transistor is illustrated in Fig. 3a and comprises a left ( $L$ ) qubit, a right ( $R$ ) qubit, and a gate. The gate is operated as one logical qubit whose state controls the operation on two qubits. Initially, the left qubit (target qubit) may be in an arbitrary state,  $|L\rangle_i = a|\uparrow\rangle + b|\downarrow\rangle$ , but the right qubit does not necessarily enjoy the same degree of freedom. Concretely, in this paper we consider  $|R\rangle_i = |\downarrow\rangle$ . The gate (the control qubit) can be configured in an ‘‘open’’ and ‘‘closed’’ state. If the gate is open, the state of the left and right qubits are interchanged,  $|L\rangle_f = |R\rangle_i$  and  $|R\rangle_f = |L\rangle_i$ . In the spin system picture, Fig. 3b, we think of this operation as a state transfer from the target  $L$  qubit to the  $R$  qubit, although the transfer is completely symmetrical. On the other hand, if the gate is closed, nothing happens,  $|L\rangle_f = |L\rangle_i$  and  $|R\rangle_f = |R\rangle_i$ . In the spin system picture, we say that the closed gate blocks the state transfer.

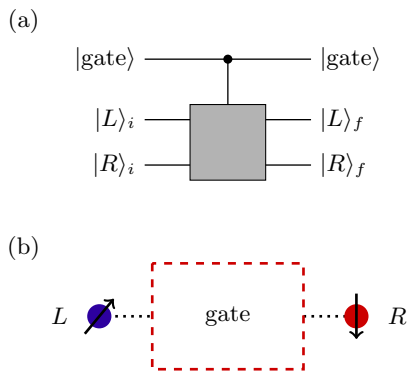


FIG. 3. The concept of a quantum transistor. (a) Schematic using gate notation. The gate state controls the operation performed on the two qubits. (b) As a spin system, one may think of two qubits ( $L$  and  $R$ ) coupled through the remainder of the spin system, called the gate.

In Ref. [29], Marchukov *et al.* showed that a linear Heisenberg spin chain of four qubits can operate as a

quantum transistor. In their design two strongly coupled qubits constitute the gate, while the left and right qubits were each coupled weakly to one of the gate qubits. The strong coupling between the gate qubits was used to detune the closed gate state from the right and left qubit states, and hence suppressing state transfer through the gate. However, since the chain was linear, there was a very small oscillating probability for transfer even when the gate was closed. Furthermore, they also found that they needed a Heisenberg XXZ chain in order to operate the transistor, i.e. different X- and Z-couplings was a key ingredient in their design.

We now seek to improve the four-qubit transistor by asking the very general question: Which conditions does a transistor functionality put on a general four-qubit system? We require the transistor to be capable of being perfectly open and closed. By ‘‘perfect’’ we mean that the open transistor shall transfer the left/right qubit states across the gate with unit fidelity (without altering the gate state), and that the closed transistor shall exhibit no dynamics at all. In this regard the model of Ref. [29] is not strictly closed. However, going beyond a simple linear chain allows for a much greater class of models.

While the initial left qubit state is arbitrary, the right qubit state is initially assumed to be spin-polarized, say, in the down-direction:

$$|L\rangle_i = a|\uparrow\rangle + b|\downarrow\rangle, \quad |a|^2 + |b|^2 = 1 \quad (1)$$

$$|R\rangle_i = |\downarrow\rangle. \quad (2)$$

Let  $|\text{open}\rangle$  and  $|\text{closed}\rangle$  be general states in the gate subspaces of total spin projection  $-1$  and  $0$ , respectively (counting up/down-spin as plus/minus one half):

$$|\text{open}\rangle = |\downarrow\downarrow\rangle \quad (3)$$

$$|\text{closed}\rangle = \cos\theta |\uparrow\downarrow\rangle + \sin\theta |\downarrow\uparrow\rangle. \quad (4)$$

With  $\theta = \pm\pi/4$  the above definitions (1)–(4) coincide with the ones in Ref. [29]. For the dynamics, we will here consider a Hamiltonian of the following type:

$$H_\diamond = J_{23}^Z \sigma_z^{(2)} \sigma_z^{(3)} + \sum_{i>j}^4 J_{ij}^X \sigma_-^{(i)} \sigma_+^{(j)} + (J_{ij}^X)^* \sigma_-^{(i)} \sigma_+^{(j)}, \quad (5)$$

where  $J_{ij}^{X,Z}$  are X,Z-coupling strengths between qubit  $i$  and  $j$ ,  $\sigma_\pm^{(i)} = (\sigma_x^{(i)} \pm i\sigma_y^{(i)})/2$  and  $\sigma_{x,y,z}^{(i)}$  are the Pauli operators for qubit  $i$ . For now we assume that the coupling strengths are real and time-independent. This model describe a Heisenberg XXZ-interaction between qubit 2 and 3, which will constitute the gate, and Heisenberg XX-interactions between all other pairs of qubits. The left and right qubits will be labeled 1 and 4, respectively. We nickname the model *the diamond model* due to the visualization in Fig. 4. Most notably, this model deviates from the one in Ref. [29] by going beyond the typically studied linear chain. This allows quantum interference between several paths between the left and right qubit to either enhance or reduce state transfer across the gate.

Contrary to the linear chain in Ref. [29], interference will allow us to close the transistor perfectly. Network Hamiltonians similar to the diamond model has been studied recently in Ref. [19] for a  $\sqrt{\text{SWAP}}$  gate, which is related to the open state of our transistor.

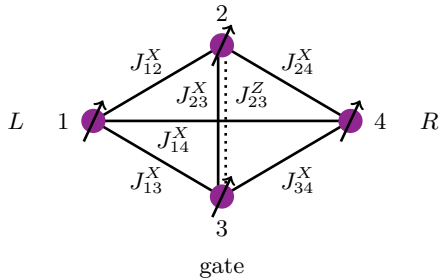


FIG. 4. Illustration of the diamond model presented in Eq (5). The purple dots with strikethrough arrows represent qubits labelled 1-4, where qubit 1 and 4 are also labelled  $L$  and  $R$ , respectively, and qubit 2 and 3 comprise the gate. The solid (dotted) lines denote X-couplings (Z-couplings), and are labelled with their strengths  $J_{ij}^{X,Z}$ .

### A. Closed transistor

When the transistor is initialized in its closed state, no dynamics in the system is allowed. This condition imposes constraints on the couplings strengths in Eq. (5). Formally, for every time  $t > 0$ , unitary time-evolution must not change the initial state<sup>1</sup>:

$$\forall t > 0: |L\rangle_i |\text{closed}\rangle |R\rangle_i \xrightarrow{t} |L\rangle_i |\text{closed}\rangle |R\rangle_i. \quad (6)$$

The full four-qubit state is denoted as a product state of those of the left qubit, the two-qubit gate and the right qubit. The condition Eq. (6) states that the initial four-qubit state must be an eigenstate of the Hamiltonian. The Hamiltonian of Eq. (5) is spin-preserving, so we consider the problem in each subspace  $\mathcal{B}_k$  of total spin projection  $k = 0, \pm 1, \pm 2$ . The initial state for the closed transistor is a linear combination of states in  $\mathcal{B}_{-1}$  and  $\mathcal{B}_0$ , namely

$$\cos \theta |\downarrow\uparrow\downarrow\downarrow\rangle + \sin \theta |\downarrow\downarrow\uparrow\downarrow\rangle \in \mathcal{B}_{-1} \quad (7)$$

$$\text{and } \cos \theta |\uparrow\uparrow\downarrow\downarrow\rangle + \sin \theta |\uparrow\downarrow\uparrow\downarrow\rangle \in \mathcal{B}_0. \quad (8)$$

Expressing the Hamiltonian of Eq. (5) as a six by six matrix in  $\mathcal{B}_0$ , we get six equations that must be fulfilled if the state in Eq. (8) is to be an eigenstate. We quickly realize that  $J_{14}^X$  must vanish, which is a reasonable requirement as this coupling connects the left and right qubits directly, allowing state transfer to bypass the gate qubits.

By requiring the state of Eq. (7) to be an eigenstate of the four by four Hamiltonian in  $\mathcal{B}_{-1}$  with the same energy as the one of Eq. (8), we get four additional equations. Comparing all the obtained equations, we find that

$$\begin{bmatrix} J_{12}^X & J_{13}^X \\ J_{13}^X & J_{12}^X \end{bmatrix} \begin{bmatrix} \cos \theta \\ \sin \theta \end{bmatrix} = \begin{bmatrix} 0 \\ 0 \end{bmatrix}. \quad (9)$$

This equation is only satisfied if  $J_{13}^X = \mp J_{12}^X$  and  $\sin \theta = \pm \cos \theta$ , i.e.  $\theta = \pm \pi/4$  as in Ref. [29]. The remaining equations imply  $J_{34}^X = \mp J_{24}^X$ . The energy of the initial state,  $|L\rangle_i |\text{closed}\rangle |R\rangle_i$ , is  $E_c = -J_{23}^Z \pm J_{23}^X$ . In total, we have reduced the number of free parameters to four coupling strengths and one sign choice.

The model derived here remains closed for more general states since even when the right qubit state is arbitrary,  $|R\rangle_i = c|\uparrow\rangle + d|\downarrow\rangle$  with  $|c|^2 + |d|^2 = 1$ , the transistor is kept closed. This means that noise on the right qubit state does not result in leakage through the gate.

### B. Open transistor

In the case of an open transistor, we wish to exchange the left and right qubit states after some time  $t_f$  of unitary time-evolution:

$$|L\rangle_i |\text{open}\rangle |R\rangle_i \xrightarrow{t_f} |R\rangle_i |\text{open}\rangle |L\rangle_i. \quad (10)$$

In the subspaces  $\mathcal{B}_{-2}$  and  $\mathcal{B}_{-1}$  this amounts to

$$\text{In } \mathcal{B}_{-2}: |\downarrow\downarrow\downarrow\downarrow\rangle \xrightarrow{t_f} |\downarrow\downarrow\downarrow\downarrow\rangle \quad (11)$$

$$\text{In } \mathcal{B}_{-1}: |\uparrow\downarrow\downarrow\downarrow\rangle \xrightarrow{t_f} |\downarrow\downarrow\uparrow\downarrow\rangle. \quad (12)$$

Since  $|\downarrow\downarrow\downarrow\downarrow\rangle$  is the only state in  $\mathcal{B}_{-2}$ , it is an eigenstate of any total-spin conserving Hamiltonian such as the one we consider. Hence, the requirement of Eq. (11) is trivially fulfilled (up to a global phase). On the other hand,  $\mathcal{B}_{-1}$  consists of four states, and the Hamiltonian in this basis is thus a four by four matrix. Comparing the time-evolved state with  $|\downarrow\downarrow\uparrow\downarrow\rangle$ , we can derive criteria the Hamiltonian need to fulfill for the transition in Eq. (12) to happen. To simplify the analytical solution, we constrain our parameters as follows: First, we pick the sign  $\theta = \pi/4$ , and hence

$$|\text{closed}\rangle = \frac{1}{\sqrt{2}}(|\uparrow\downarrow\rangle + |\downarrow\uparrow\rangle). \quad (13)$$

Next, we impose left/right symmetry in the parameters:  $J_{12}^X = J_{24}^X = -J_{13}^X = -J_{34}^X$ . Finally, simulations show that  $J_{23}^X$  cause unwanted interference in the state transfer, so we set  $J_{23}^X = 0$ . A sketch of this reduced model with merely two parameters  $J_{23}^Z$  and  $J_{12}^X$ , both assumed non-zero, is shown in Fig. 5.

With these simplifications, we can find simple expressions for the eigenstates and eigenenergies of the four

<sup>1</sup> Of course, the four-qubit state will acquire an overall phase factor, but this does not change the state.

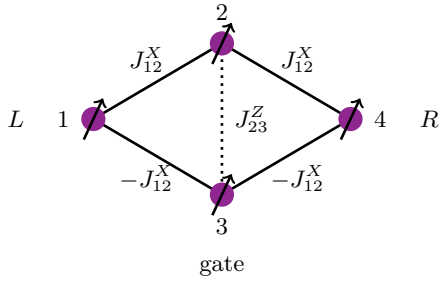


FIG. 5. Illustration of the four-qubit diamond model with notation explained in the caption of Fig. 4. Under the condition of Eq. (16) this model functions as a quantum transistor.

by four Hamiltonian in the subspace  $\mathcal{B}_{-1}$ . The non-normalized eigenstates are

$$\begin{aligned} |E_1\rangle &= |\uparrow\downarrow\downarrow\downarrow\rangle + |\downarrow\downarrow\uparrow\downarrow\rangle, \\ |E_2\rangle &= |\downarrow\downarrow\downarrow\uparrow\rangle - |\uparrow\downarrow\downarrow\downarrow\rangle, \\ |E_3\rangle &= |\uparrow\downarrow\downarrow\downarrow\rangle - \zeta|\uparrow\downarrow\downarrow\downarrow\rangle + \zeta|\downarrow\downarrow\uparrow\downarrow\rangle + |\downarrow\downarrow\downarrow\uparrow\rangle, \\ |E_4\rangle &= |\uparrow\downarrow\downarrow\downarrow\rangle + \zeta^{-1}|\uparrow\downarrow\downarrow\downarrow\rangle - \zeta^{-1}|\downarrow\downarrow\uparrow\downarrow\rangle + |\downarrow\downarrow\downarrow\uparrow\rangle, \end{aligned} \quad (14)$$

where  $\zeta = (J_{23}^Z + L)/2J_{12}^X$  with  $L = \sqrt{4(J_{12}^X)^2 + (J_{23}^Z)^2}$ , and the energies are  $E_1 = -J_{23}^Z$ ,  $E_2 = +J_{23}^Z$ ,  $E_3 = -L$  and  $E_4 = +L$ . In the basis of eigenstates, we may express the states

$$\begin{aligned} |\uparrow\downarrow\downarrow\downarrow\rangle &= -\frac{|E_2\rangle}{\langle E_2|E_2\rangle} + \frac{|E_3\rangle}{\langle E_3|E_3\rangle} + \frac{|E_4\rangle}{\langle E_4|E_4\rangle} \\ |\downarrow\downarrow\downarrow\uparrow\rangle &= +\frac{|E_2\rangle}{\langle E_2|E_2\rangle} + \frac{|E_3\rangle}{\langle E_3|E_3\rangle} + \frac{|E_4\rangle}{\langle E_4|E_4\rangle}, \end{aligned} \quad (15)$$

and note here that the only difference is the sign on the first term. Thus the  $|\uparrow\rangle$  state at the left qubit position is transferred to the right qubit port with unity fidelity in time  $t_f$  if and only if the time-evolution flips the relative sign between  $|E_2\rangle$  and the states  $|E_3\rangle$  and  $|E_4\rangle$ , i.e.  $e^{-i(E_2-E_3)t_f} = e^{-i(E_2-E_4)t_f} = -1$ . Solving these equations, we find the transfer time as  $t_f = \pi/|J_{23}^Z|^2$  and a criterion on the ratio of coupling strengths, similar to the one found in e.g. Ref. [56],

$$\left| \frac{J_{12}^X}{J_{23}^Z} \right| = \sqrt{m^2 - \frac{1}{4}}, \quad m = 1, 2, 3, \dots, \quad (16)$$

the simplest case ( $m = 1$ ) yielding  $J_{12}^X = \pm\sqrt{3/4}J_{23}^Z$ .

During the state transfer in Eq. (12), the state  $|\downarrow\downarrow\downarrow\downarrow\rangle$ , being an eigenstate with energy  $J_{23}^Z$ , accumulates a phase factor  $e^{-i\pi} = -1$ . Thus, the initial state evolves,

$$\begin{aligned} |L\rangle_i |\text{open}\rangle |R\rangle_i &= (a|\uparrow\rangle + b|\downarrow\rangle)|\downarrow\downarrow\rangle|\downarrow\rangle \\ &\xrightarrow{t_f} |\downarrow\rangle|\downarrow\rangle(a|\uparrow\rangle - b|\downarrow\rangle). \end{aligned} \quad (17)$$

<sup>2</sup> The state transfer occurs periodically at any odd integer multiple of  $t_f$ , but we are merely interested in the first instance.

So in order to achieve the total state transfer suggested in Eq. (10), we must apply a single-qubit phase gate on the right qubit to fix the sign, an operation which can be done in zero time [57]. This is a simple task, and we conclude that the diamond model is capable of functioning as a quantum transistor.

One may wonder whether the open transistor works for an arbitrary right qubit state, as in the case of the closed transistor. This would indeed be the case if  $|\uparrow\downarrow\downarrow\rangle$  was an eigenstate, but it is not, and such a term in the initial state becomes a non-trivial state in  $\mathcal{B}_0$  as time passes. Therefore, we can not relax the requirement  $|R\rangle_i = |\downarrow\rangle$ . If the transistor was able to operate with an arbitrary initial right qubit state, it would constitute a conditional swap operation on two arbitrary left and right qubit states [58, 59]. Such a gate, called CSWAP or Fredkin gate, is universal for quantum computing, and a simple realization of this gate is much-coveted. However, we speculate that the CSWAP could be possible if we promote the two gate qubits to qutrits (three-level systems), thereby extending the Hilbert space, giving more degrees of freedom for a complete Fredkin gate.

### III. TOWARDS AN IMPLEMENTATION WITH SUPERCONDUCTING CIRCUITS

In the previous section, we saw that a four-qubit system with Heisenberg interactions could function as a quantum transistor. We kept the model simple in order to gain analytical insight. Now, we use the simple model as a stepping stone towards a more realistic case, and consider how such a diamond transistor may be realized in a real physical system, specifically in superconducting circuits.

We consider the spin Hamiltonian to be

$$H_0 = \frac{1}{2}(\Omega + \Delta)(\sigma_z^{(1)} + \sigma_z^{(4)}) + \frac{1}{2}\Omega(\sigma_z^{(2)} + \sigma_z^{(3)}), \quad (18)$$

where  $\Delta$  denote a detuning of qubit 1 (left qubit) and qubit 4 (right qubit) from the frequency  $\Omega$  of qubits 2 and 3 (the gate qubits). For the interaction part, we consider:

$$\begin{aligned} H_{\text{int}} &= J_z\sigma_z^{(2)}\sigma_z^{(3)} + J_x\sigma_x^{(2)}\sigma_x^{(3)} \\ &\quad + J_2(\sigma_x^{(1)} + \sigma_x^{(4)})(\sigma_x^{(2)} - \sigma_x^{(3)}). \end{aligned} \quad (19)$$

These type of interaction terms are naturally realized with superconducting circuits. Assuming  $|2\Omega + \Delta| \gg |\Delta|$ , we employ the rotating wave approximation and ignore the fastest oscillating terms, such that the system Hamiltonian in the frame rotating with  $H_0$  becomes:

$$\begin{aligned} H &= J_z\sigma_z^{(2)}\sigma_z^{(3)} + J_x(\sigma_+^{(2)}\sigma_-^{(3)} + \sigma_-^{(2)}\sigma_+^{(3)}) \\ &\quad + J_2(\sigma_+^{(1)} + \sigma_+^{(4)})(\sigma_-^{(2)} - \sigma_-^{(3)})e^{i\Delta t} \\ &\quad + J_2(\sigma_-^{(1)} + \sigma_-^{(4)})(\sigma_+^{(2)} - \sigma_+^{(3)})e^{-i\Delta t}. \end{aligned} \quad (20)$$

Notice that this model, sketched in Fig. 6, is a special case of the diamond model defined in Eq. (5). In fact,

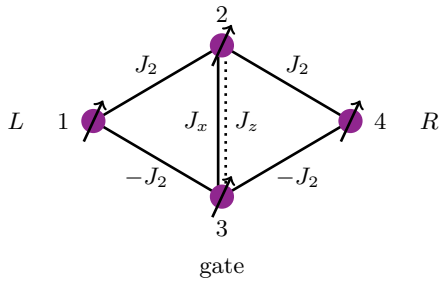


FIG. 6. Illustration of the diamond model we wish to implement using superconducting qubits, given as  $H$  in Eq. (20). Notation on the figure is explained in the caption of Fig. 4.

if we set  $\Delta = J_x = 0$  and  $J_2 = \pm\sqrt{3/4}J_z$ , the model reduces to the final model of the previous section.

From the previous section, we readily observe that the model functions as an closed transistor. The model also function as an open transistor as we will show here. The detuning  $\Delta$  between the gate qubits and the left/right qubits results in a time-oscillating coupling. We solve the time-evolution analytically using the Floquet formalism [60], and the transfer time can then be determined in a similar way to what was done in Section II B. Under the assumption that the detuning is much larger than the qubit-qubit-couplings, which is typical for superconducting qubits, the transfer time is given as (see Appendix A):

$$t_f = \frac{\pi|\Delta|}{4J_2^2}, \quad (21)$$

with the process being essentially transfer through a second-order Raman transition with the coupling  $\sim 4J_2^2/\Delta$ . Remarkably, nearly perfect state transfer is achieved no matter the exact values of the detuning  $\Delta \sim 2\pi$  GHz, the qubit-qubit coupling  $J_2$ , the Z-coupling  $J_z$  and X-coupling  $J_x$ . This should be contrasted to the resonant case ( $\Delta = 0$ ), where state transfer is conditioned to the parameter constraint of Eq. (16). When strong driving is applied through  $\Delta$ , this parameter constraint is relaxed to the condition that  $G \equiv (J_x + 2J_z)\Delta/8J_2^2$  should be an integer. However, since  $\Delta$  is typically three orders of magnitude larger than the  $J$ 's,  $G$  is a large number that can be well-approximated by the nearest integer with only a small relative error. Thus, we may consider the condition approximately fulfilled, and nearly perfect state transfer is always achieved (see Appendix A for details).

We also note a few observations about the transfer time of Eq. (21). Firstly, state transfer is suppressed (large  $t_f$ ) when either the detuning  $\Delta$  becomes large or coupling  $J_2$  becomes weak, both of which effectively decouple the left/right qubits and the gate. Secondly, the transfer time is independent of the gate couplings  $J_x$  and  $J_z$ , suggesting that these couplings do not take an active part in the state transfer. This should also be contrasted to the resonant case, where the transfer time is given entirely by the Z-coupling in the gate, it being the only energy scale

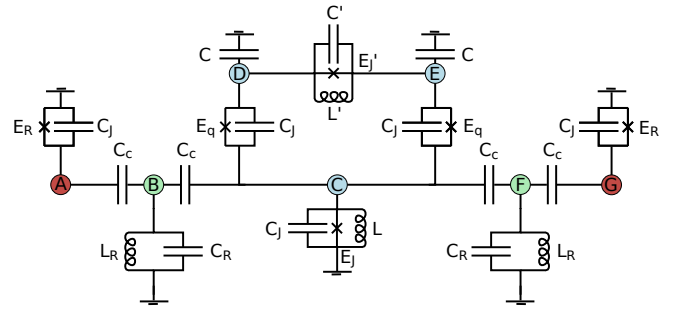


FIG. 7. Circuit diagram for the circuit that implements the Hamiltonian of Eq. (22). Each circuit element has been labeled with its properties, so that the capacitors are labeled with their capacitances  $C, C_c, C_J, C', C_R$ , the inductors with their inductances  $L, L', L_R$  and the Josephson junctions by their Josephson energies  $E_J, E'_J, E_q, E_R$ . Each node in the circuit is labeled by a letter A-G.

of the system.

#### IV. NUMERICAL SIMULATIONS

As already mentioned, we wish to implement the diamond model of Eq. (20) using superconducting qubits. We claim that the superconducting circuit in Fig. 7<sup>3</sup> will do the job. In addition to the couplings in Eq. 20, we also get an unwanted coupling between the left and right qubit so that the Hamiltonian implemented by the circuit is:

$$\begin{aligned} H = & J_z \sigma_z^{(2)} \sigma_z^{(3)} + J_x (\sigma_+^{(2)} \sigma_-^{(3)} + \sigma_-^{(2)} \sigma_+^{(3)}) \\ & + J_2 (\sigma_+^{(1)} + \sigma_+^{(4)}) (\sigma_-^{(2)} - \sigma_-^{(3)}) e^{i\Delta t} \\ & + J_2 (\sigma_-^{(1)} + \sigma_-^{(4)}) (\sigma_+^{(2)} - \sigma_+^{(3)}) e^{-i\Delta t} \\ & + J_4 (\sigma_+^{(1)} \sigma_-^{(4)} + \sigma_-^{(1)} \sigma_+^{(4)}). \end{aligned} \quad (22)$$

As we remarked in Section II A, the cross-talk term of strength  $J_4$  allows state transfer to bypass the gate, resulting in a leaking closed transistor. Fortunately, we can suppress this coupling by making the capacitance  $C_R$  large, which lowers the resonance frequency of the coupling resonator. Details on the analysis of the circuit and expressions for the parameters in the Hamiltonian in terms of circuit parameters are provided in Appendix B.

In this section we wish to study the performance of the diamond transistor in a realistic setting. Our simulations is therefore based on the Hamiltonian of Eq. (22) where the parameters are found from realistic circuit parameters using the relationships in Appendix B. An experimental realization of the system will necessarily introduce noise,

<sup>3</sup> A patent application pertaining to the circuit, and the XXZ gate in particular, has been filed with the European Patent Office (application number 17185721.2 - 1879).

TABLE I. Circuit parameters and corresponding spin model parameters.

Panel A: Circuit parameters appearing in Fig. 7											
$L/\text{nH}$	$L'/\text{nH}$	$L_R/\text{nH}$	$\frac{E_J}{2\pi\text{GHz}}$	$\frac{E'_J}{2\pi\text{GHz}}$	$\frac{E_q}{2\pi\text{GHz}}$	$\frac{E_R}{2\pi\text{GHz}}$	$C/\text{fF}$	$C_J/\text{fF}$	$C'/\text{fF}$	$C_c/\text{fF}$	$C_R/\text{fF}$
20	2	20	38	38	15	41	91	20	47	17	2000
Panel B: Effective energy ratios and spin model parameters											
$E_{J,1}/E_{C,1}$	$E_{J,2}/E_{C,2}$	$E_{L,2}/E_{J,2}$	$\Omega/2\pi\text{GHz}$	$\Delta/2\pi\text{GHz}$	$J_z/2\pi\text{MHz}$	$J_x/J_z$	$J_2/J_z$	$J_4/J_z$			
78.01	50.10	0.9556	-13.67	1.067	-41.99	0.8690	0.3003	$-9.898 \cdot 10^{-4}$			

and so we include realistic dephasing noise in the simulations, too. We do not consider spin flip noise, which could potentially flip between the open and closed gate, since the closed flux loop inherent to the gate will likely make flux noise dominant[39].

Specifically, we use the spin model parameters in Panel B of Table I. This set of parameters is found from the circuit parameters in Panel A. We stress that we did not fine-tune any of the parameters in Table I, and that the transistor properties reported in this section are inherent to the diamond model.

Note that the energy ratios  $E_{J,i} \gg E_{C,i}$  suitable for transmon qubits ( $i = 1, 2$ ), and  $E_{L,2} \sim E_{J,2}$ . Also note that  $C_R$  has been chosen large to suppress the unwanted cross-talk of strength  $J_4$  such that the gate can be closed effectively on the time-scale of operation.

### A. Time-evolution and transition fidelities

To model decoherence in the system from dephasing noise, we consider the Lindblad master equation,

$$\dot{\rho} = -i[H, \rho] + \sum_{i=1}^4 \gamma_i \left[ \sigma_z^{(i)} \rho \sigma_z^{(i)} - \frac{1}{2} (\rho(\sigma_z^{(i)})^2 + (\sigma_z^{(i)})^2 \rho) \right], \quad (23)$$

with  $\rho$  the density matrix,  $H$  the Hamiltonian of Eq. (22) and  $\sqrt{\gamma_i} \sigma_z^{(i)}$  the collapse operator causing phase flip of qubit  $i$ , and  $\gamma_i$  being the corresponding rate. We set  $\gamma_1 = \gamma_4 = \gamma_2/2 = \gamma_3/2 \equiv \gamma$ , modeling shorter decoherence time on gate than the left/right qubits. State-of-the-art values for the decoherence rate are  $\gamma/2\pi \sim 0.01 \text{ MHz}/2\pi = 0.0016 \text{ MHz}$ , corresponding to the time-scale  $1/\gamma \sim 100 \mu\text{s}$ . As we will see, decoherence plays a role on a time-scale two order of magnitude magnitudes larger than the operation time of the transistor, and is not considered an eminent threat to our protocol.

In order to determine the time-evolution of a pure state,  $|L\rangle_i |\text{gate}\rangle |R\rangle_i$ , we employ the Python toolbox QuTiP[61] to solve Eq. (23). The state fidelity of a transition from the initial state  $|i\rangle$ , encoded in  $\rho(0)$ , to the desired final state  $|f\rangle$  is defined as:

$$F_{i \rightarrow f}(t) \equiv \text{Tr}(\rho(t)|f\rangle\langle f|). \quad (24)$$

The fidelity is a measure of how probable it is to find the

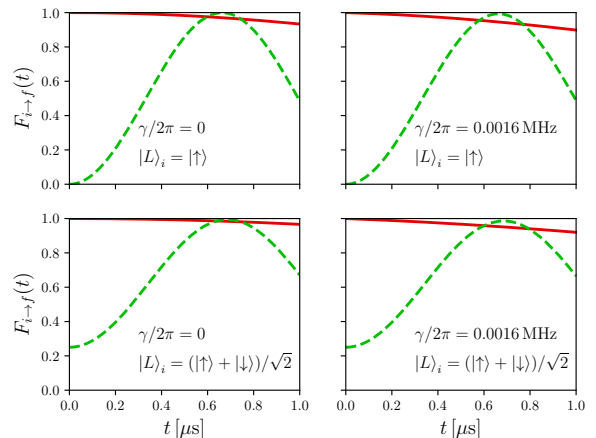


FIG. 8. State transfer fidelities as a function of time calculated from Eq. (24) for a closed (solid red) and open gate (dashed green). The considered transitions for either case are described in the main text. The upper two panels use the left qubit initial state  $|L\rangle_i = |\uparrow\rangle$ , while the lower two use  $|L\rangle_i = (|\uparrow\rangle + |\downarrow\rangle)/\sqrt{2}$ . Decoherence noise is included only in the right panels with rate  $\gamma/2\pi = 0.0016 \text{ MHz}$ . The spin model parameters are given in Table I.

transistor in the desired final state, and we will use it to evaluate how well the transistor functions.

Even though the transistor is expected to work for arbitrary initial left qubit states, we will for concreteness take it to be either  $|L\rangle_i = |\uparrow\rangle$  or  $|L\rangle_i = \frac{1}{\sqrt{2}}(|\uparrow\rangle + |\downarrow\rangle)$ . These choices allow us to study both a spin-polarized state and a superposition state.<sup>4</sup> The right qubit is initialized according to Eq. (2), and the gate is either open or closed, as defined in Eqs. (3) and (13).

We show the simulation results in Fig. 8 for the aforementioned initial left qubit states (horizontal split) and with/without dephasing noise (vertical split).

Due to the accumulated sign difference of  $|\uparrow\downarrow\downarrow\rangle$  and  $|\downarrow\downarrow\downarrow\rangle$  observed in Section II, we will define the fidelity using the transition in Eq. (17). The fidelity for this

<sup>4</sup> We avoid  $|L\rangle_i = |\downarrow\rangle$  since, in the case of an open gate we get the eigenstate  $|\downarrow\downarrow\downarrow\rangle$  and trivial state transfer.

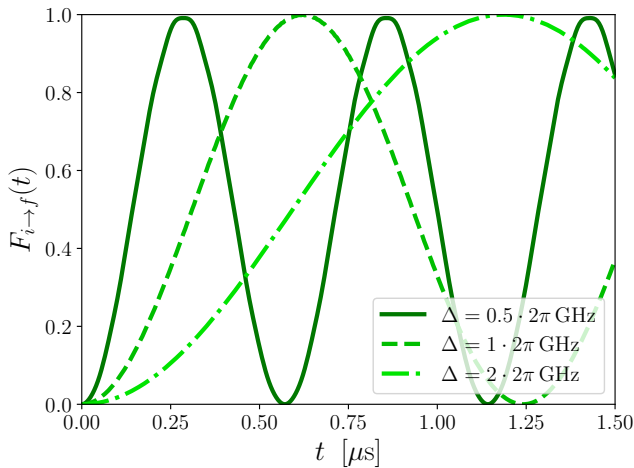


FIG. 9. State transfer fidelities as a function of time calculated from Eq. (24) for an open gate with the initial left qubit state  $|L\rangle_i = |\uparrow\rangle$  and no decoherence. The three plots are made with various detuning frequencies  $\Delta$ , and all remaining parameters taken from Table I.

transition is shown as the dashed green lines on Figure 8. Notice that it almost reaches unity just before  $0.7 \mu\text{s}$ . The transfer fidelity is only barely reduced by dephasing noise. In fact, the transfer time is faster than the analytic prediction of  $0.84 \mu\text{s}$  computed from Eq. (21), which is consistent with the effect of the additional small cross-talk term.

When the gate is closed, we compute the fidelity with the final state set equal to the initial one. The fidelities for this non-transition are shown as the solid red lines in Fig. 8. Due to a non-zero cross-talk term,  $J_4 \neq 0$ , the gate is prone to leak slightly over time, and, not surprisingly, decoherence speeds up the process. However, during the operation of the open gate ( $\sim 0.7 \mu\text{s}$ ), the transistor remains well-closed,  $F_{i \rightarrow f} > 0.95$ .

Another analytic prediction for the transfer time is its scaling with  $|\Delta|$  and  $J_2^{-2}$ . Simulations verify this behavior very accurately. In reality  $\Delta$  and  $J_2$  cannot be changed independently since they are connected through the circuit parameters. However, in order to single-out the role of  $\Delta$  and illustrate its role in the transfer time, we show in Fig. 9 the fidelity for the open gate with various values of  $\Delta$  and the remaining spin model parameters fixed. Besides illustrating the tunability of the transfer time, this result clearly demonstrates that the state transfer is perfect or nearly perfect no matter the exact parameter values, rendering the transistor properties very robust.

## B. State preparation

In order to operate the transistor successively, we need a scheme for preparing the state of the input qubit and the gate. It is advantageous if we can address the gate qubits exclusively, in which case the gate may be switched

on or off independently of the left and right qubits. This is the case if the left/right qubits are far detuned from the gate qubits, i.e. when  $\Delta$  is sufficiently large. Since  $\Delta \sim 2\pi \text{ GHz}$ , we may address the gate qubits with microwave radiation without affecting the input and output qubits. In experiments, the input and output frequencies may be tuned in situ using flux control lines.

Next we need to ensure that the gate can be opened and closed in a controlled way. Suppose we start in the open gate state, and we wish to close the gate, or the opposite. This can be achieved by driving the nodes  $D$  and  $E$  on the circuit in Fig. 7, thereby introducing the following additional term in the interaction-picture Hamiltonian:

$$H_d(t) = iA \cos(\omega_d t) \times \left[ (\sigma_+^{(2)} + \sigma_+^{(3)})e^{i\Omega t} + (\sigma_-^{(2)} + \sigma_-^{(3)})e^{-i\Omega t} \right]. \quad (25)$$

This driving term, like the remaining Hamiltonian, preserves the total spin, thus starting from any of the triplet states shown in Fig. 10, we can ignore the singlet state  $(|\uparrow\downarrow\rangle - |\downarrow\uparrow\rangle)/\sqrt{2}$ . The driving introduces Rabi oscillations between the closed and open states, provided the driving frequency matches the energy difference,  $\omega_d = |\Omega - 3J_z|$ , and  $A \ll J_z$ . Thus starting from  $|\text{open}\rangle$  (or  $|\text{closed}\rangle$ ) a  $\pi$ -pulse,  $\omega_d t = \pi$ , would kick the gate state to  $|\text{closed}\rangle$  (or  $|\text{open}\rangle$ ) in about  $0.05 \mu\text{s}$ . With  $J_z \sim -30 \cdot 2\pi \text{ MHz}$  the energy difference between the open or closed state and  $|\uparrow\uparrow\rangle$  are far enough from  $\omega_d$  as to not accidentally populate  $|\uparrow\uparrow\rangle$ . Using the mechanism described here, we can therefore switch between the open and closed transistor with a simple external microwave drive.

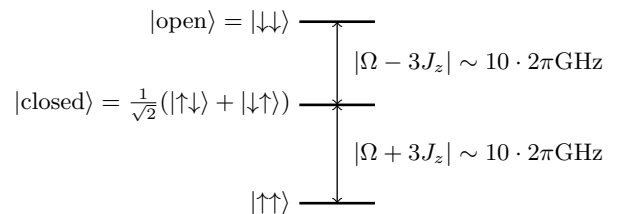


FIG. 10. Sketch of the triplet gate states, typical parameters are  $\Omega \sim -10 \cdot 2\pi \text{ GHz}$  and  $J_z \sim -30 \cdot 2\pi \text{ MHz}$ .

## V. CONCLUSIONS AND OUTLOOK

We have discussed the notion of a quantum transistor, and introduced a model for such a device comprised of four qubits interacting via Heisenberg XX and Heisenberg XXZ couplings. Using basic quantum mechanics and Floquet theory, we showed that our ‘diamond model’ is capable of operating as a transistor without fine-tuning the spin model parameters. Then we proposed a concrete implementation of the model as a superconducting circuit, and demonstrated its capability of operating with high-fidelity in a realistic noisy setting. Seeking a compromise

between fast state transfer and a well-closed gate, we simulated the transistor with one example circuit parameter choice.

Our proposed transistor model is readily implementable in state-of-the-art experiments with superconducting qubits, and may serve as a vital ingredient in larger networks for quantum computation. In fact, the transistor is very closely related to the Fredkin gate (CSWAP), which is a universal gate for quantum computing, i.e. a network of Fredkin gates could perform any quantum computation. The Fredkin gate exchanges two arbitrary qubit states conditioned by the value of a control qubit, and consequently we may regard our transistor as a Fredkin gate, where one of these swapped qubits is not arbitrary, but restricted to the  $|\downarrow\rangle$  state.

### ACKNOWLEDGMENTS

We thank D. Petrosyan and O. V. Marchukov for many inspiring discussions about the concept of a quantum spin transistor, and we thank T. Bækkegaard, A. G. Volosniev, and M. Valiente for discussions and comments on different aspects of the work. We thank W. D. Oliver, S. Gustavsson, and M. Kjørgaard from the Engineering Quantum Systems Group at MIT for their kind hospitality and for extended discussion on superconducting circuits. This work was supported by the Carlsberg Foundation and the Danish Council for Independent Research under the DFF Sapere Aude program.

### Appendix A: Driven system

Consider the periodically driven time-dependent Hamiltonian of Eq. (20), which can be cast as

$$H = H_0 + H_1 e^{i\Delta t} + H_1^\dagger e^{-i\Delta t}, \quad (\text{A1})$$

with

$$\begin{aligned} H_0 &= J_z \sigma_z^{(2)} \sigma_z^{(3)} + J_x (\sigma_+^{(2)} \sigma_-^{(3)} + \sigma_-^{(2)} \sigma_+^{(3)}) \\ H_1 &= J_2 (\sigma_+^{(1)} + \sigma_+^{(4)}) (\sigma_-^{(2)} - \sigma_-^{(3)}). \end{aligned} \quad (\text{A2})$$

We now wish to analyze the open gate: see whether perfect or near-perfect state transfer is possible and, if so, find an expression for the transfer time. Floquet theory is developed to treat such periodically driven systems, and the time-evolution operator can be expressed as an exponential of a Floquet Hamiltonian. For typical parameter values in superconducting qubits, the driving frequency  $\Delta \sim 2\pi$  GHz is about a thousand times larger than the energy scale set by  $J_z$ ,  $J_x$  and  $J_2$ . In other words: While the open gate permits one cycle of state transfer, the driving terms in the Hamiltonian has undergone a thousand oscillations. So it is appropriate to compute the Floquet Hamiltonian using an inverse-frequency expansion known as the Magnus expansion[60]. To first order in  $\Delta^{-1}$ , the

Magnus expansion states that the (stroboscopic) Floquet Hamiltonian can be expressed as

$$H_F = H_0 + \frac{1}{\Delta} \left( [H_1, H_1^\dagger] - [H_1, H_0] + [H_1^\dagger, H_0] \right). \quad (\text{A3})$$

After some Pauli operator gymnastics we find:

$$\begin{aligned} [H_1, H_1^\dagger] &= + J_2^2 (\sigma_-^{(2)} \sigma_+^{(2)} + \sigma_-^{(3)} \sigma_+^{(3)}) (\sigma_z^{(1)} + \sigma_z^{(4)}) \\ &\quad - J_2^2 (\sigma_-^{(2)} \sigma_+^{(3)} + \sigma_+^{(2)} \sigma_-^{(3)}) (\sigma_z^{(1)} + \sigma_z^{(4)}) \\ &\quad - J_2^2 (\sigma_-^{(1)} \sigma_+^{(1)} + \sigma_-^{(4)} \sigma_+^{(4)}) (\sigma_z^{(2)} + \sigma_z^{(3)}) \\ &\quad - J_2^2 (\sigma_-^{(1)} \sigma_+^{(4)} + \sigma_+^{(1)} \sigma_-^{(4)}) (\sigma_z^{(2)} + \sigma_z^{(3)}) \\ [H_1, H_0] &= J_2 \tilde{J} (\sigma_-^{(2)} \sigma_z^{(3)} - \sigma_-^{(3)} \sigma_z^{(2)}) (\sigma_+^{(1)} + \sigma_+^{(4)}) \\ [H_1^\dagger, H_0] &= - [H_1, H_0]^\dagger, \end{aligned} \quad (\text{A4})$$

where we have defined  $\tilde{J} = 2J_z + J_x$  for later convenience.

The operator  $U(T, 0) = e^{-iH_F T}$  takes the system from time zero through one driving cycle of period  $T = 2\pi\Delta^{-1}$ . Therefore, successive application of this operator  $n$  times,

$$U(nT, 0) = e^{-iH_F nT}, \quad (\text{A5})$$

will take the system from time zero to time  $nT$ . Since the driving period  $T$  is very small compared to the state transfer time, we will consider  $t = nT$  a continuous time-variable.

The Floquet Hamiltonian  $H_F$ , like  $H$ , conserves the total spin projection. So, as we are interested in the time-evolution of  $|\uparrow\downarrow\downarrow\rangle$ , it suffices to diagonalize  $H_F$  in the subspace  $\mathcal{B}_{-1}$ . The (non-normalized) eigenstates have the same form as in the non-driven case studied in the main text:

$$\begin{aligned} |E_1\rangle &= |\downarrow\uparrow\downarrow\downarrow\rangle + |\downarrow\downarrow\uparrow\downarrow\rangle, \\ |E_2\rangle &= |\downarrow\downarrow\uparrow\uparrow\rangle - |\uparrow\downarrow\downarrow\downarrow\rangle, \\ |E_3\rangle &= |\uparrow\downarrow\downarrow\downarrow\rangle - \tilde{\zeta} |\downarrow\uparrow\downarrow\downarrow\rangle + \tilde{\zeta} |\downarrow\downarrow\uparrow\downarrow\rangle + |\downarrow\downarrow\downarrow\uparrow\rangle, \\ |E_4\rangle &= |\uparrow\downarrow\downarrow\downarrow\rangle + \tilde{\zeta}^{-1} |\downarrow\uparrow\downarrow\downarrow\rangle - \tilde{\zeta}^{-1} |\downarrow\downarrow\uparrow\downarrow\rangle + |\downarrow\downarrow\downarrow\uparrow\rangle, \end{aligned} \quad (\text{A6})$$

where  $\tilde{\zeta}$  is a very complicated function of  $J_2$ ,  $J_x$ ,  $J_z$  and  $\Delta$  whose exact form is irrelevant for our analysis. The energies are  $E_1 = J_x - J_z$ ,  $E_2 = J_z$ ,  $E_3 = -(J_x + \kappa)/2$  and  $E_4 = -(J_x - \kappa)/2$ , with

$$\kappa = \sqrt{\frac{64J_2^4}{\Delta^2} + \frac{16J_2^2 \tilde{J}(\tilde{J} + \Delta)}{\Delta^2}} + \tilde{J}^2. \quad (\text{A7})$$

Just like in simple case studied in the main text, we may expand the following states in the eigenbasis:

$$\begin{aligned} |\uparrow\downarrow\downarrow\downarrow\rangle &= -\frac{|E_2\rangle}{\langle E_2|E_2\rangle} + \frac{|E_3\rangle}{\langle E_3|E_3\rangle} + \frac{|E_4\rangle}{\langle E_4|E_4\rangle} \\ |\downarrow\downarrow\downarrow\uparrow\rangle &= +\frac{|E_2\rangle}{\langle E_2|E_2\rangle} + \frac{|E_3\rangle}{\langle E_3|E_3\rangle} + \frac{|E_4\rangle}{\langle E_4|E_4\rangle}. \end{aligned} \quad (\text{A8})$$

So the  $|\uparrow\rangle$  state is transferred from the left to the right position when unitary time evolution accounts for the

relative sign between  $|E_2\rangle$  and the states  $|E_3\rangle$  and  $|E_4\rangle$ , i.e.  $e^{-i(E_2-E_3)t_f} = e^{-i(E_2-E_4)t_f} = -1$ . This is equivalently expressed as

$$\begin{cases} (E_2 - E_3)t_f = (2n + 1)\pi \\ (E_2 - E_4)t_f = (2m + 1)\pi \end{cases} \quad (\text{A9})$$

$$\Leftrightarrow \begin{cases} (\tilde{J} + \kappa)t = 2(2n + 1)\pi \\ (\tilde{J} - \kappa)t = 2(2m + 1)\pi \end{cases} \quad (\text{A10})$$

for  $n, m \in \mathbb{Z}$ .

If  $\tilde{J} = 0$ , then  $\kappa = 8J_2^2/|\Delta|$  and the conditions in Eq. (A10) reduces to a single equation. Seeking the solution for the smallest positive  $t_f$  yields the transfer time:

$$t_f = \frac{\pi|\Delta|}{4J_2^2} \quad (\tilde{J} = 0). \quad (\text{A11})$$

If  $\tilde{J} \neq 0$ , we can simplify  $\kappa$  by taking the limit  $|\tilde{J}|, |J_2| \ll |\Delta|$ . Neglecting term  $\sim \Delta^{-2}$  in the square root, Eq. (A7) becomes

$$\kappa \approx \sqrt{\frac{16J_2^2\tilde{J}}{\Delta} + \tilde{J}^2} \approx |\tilde{J}| \left( \frac{8J_2^2}{\Delta\tilde{J}} + 1 \right), \quad (\text{A12})$$

where the last approximation is a first order expansion of the square root. With the above approximation for  $\kappa$ , we see that the two conditions in Eq. (A10) define two time-scales,  $(\tilde{J} \pm \kappa)^{-1}$ : one short  $\sim \tilde{J}^{-1}$  and one much longer  $\sim \Delta/J_2^2$ . The long time-scale will set the speed limit for the state transfer, and it will fulfill the state transfer condition for the first time when

$$\left| -\frac{8J_2^2}{\Delta} \right| t_f = 2\pi \Leftrightarrow t_f = \frac{\pi|\Delta|}{4J_2^2} \quad (\tilde{J} \neq 0). \quad (\text{A13})$$

During this transfer time, the state transfer condition derived from the short time-scale is satisfied  $\sim 100$  times, so in practice this condition will also be satisfied at, or very close to, the transfer time of Eq. (A13). Technically, we find the constraint that  $\tilde{J}\Delta/8J_2^2$  must be an integer, but since its magnitude is very large, it may be very well approximated by the nearest integer and the constraint consider fulfilled. So, for both zero and non-zero  $\tilde{J}$ , we find that (nearly) perfect state transfer is achieved in time

$$t_f = \frac{\pi|\Delta|}{4J_2^2}. \quad (\text{A14})$$

## Appendix B: Implementation with superconducting circuits

In this section the units  $2e$  and  $\Phi_0/2\pi$  are kept explicitly. We see in Fig. 7 a circuit that will implement the diamond Heisenberg model in Eq. 22. The goal of this appendix is to indicate how the implementation works and provide

expressions for the parameters in the Hamiltonian in terms of properties of the circuit elements that make up the circuit. To do this, we will model the transmission-line resonators as LC-circuits with capacitances  $C_R$  and inductances  $L_R$ . For each node in the circuit, labelled  $A, B, \dots, G$  in Fig. 7, we have a related flux degree of freedom. Denoting the flux degree of freedom at node  $i$  by  $\phi_i$ , we have the seven degrees of freedom  $\phi_A, \phi_B, \dots, \phi_G$ . It is however more advantageous to describe the circuit in terms of the variables

$$\begin{aligned} \phi_1 &= \phi_A \\ \phi_2 &= \phi_D - \phi_E - \phi_C \\ \phi_3 &= \phi_D - \phi_E + \phi_C \\ \phi_4 &= \phi_G \\ \phi_{LR} &= \phi_B \\ \phi_{RR} &= \phi_F \\ \phi_{CM} &= \phi_C + \phi_D + \phi_E. \end{aligned} \quad (\text{B1})$$

Once the system is quantized, each of the four numbered fluxes will correspond to the qubit in Fig. 6 of the same number. Note that the two left/right qubits reside in the two transmon qubits in the far left/right of the circuit in Fig. 7, while the two gate qubits consist of linear combinations of the fluxes  $C, D, E$  of the inner part of the circuit. The advantages of this choice of coordinates is threefold. First of all, it implements the  $\sigma_z^{(2)}\sigma_z^{(3)}$  coupling between the two gate qubits. Second, it guarantees that the couplings between the gate qubits and left/right qubits are anti-symmetric with respect to permutation of qubit 2 and 3 (seen in Fig. 6) as long as the circuit is built symmetrically. Finally, the fact that the left/right qubits are just two transmon qubits at the edge of the circuit should mean the circuit is relatively easy to integrate into larger architectures.

The remaining three coordinates are a center of mass-like coordinate  $\phi_{CM}$  and the two resonator-fluxes  $\phi_{LR}$  and  $\phi_{RR}$ , corresponding to the left and right resonator respectively. These degrees of freedom can be detuned sufficiently through parameter choices that they do not couple significantly to the numbered qubits, and hence can be ignored in the following. Nevertheless, the fact that the coupling between the left/right and gate qubits occurs indirectly through the resonators plays an important role in controlling the strengths of these couplings, as we will later see.

Having established the important degrees of freedom, the analysis of the circuit is now a relatively straightforward calculation. What is found is that the four degrees of freedom  $\phi_1, \phi_2, \phi_3$  and  $\phi_4$  each support a qubit, with the energy spacing between the two states of the qubits being identical between the two gate qubits and between the two left/right qubits. Interactions are induced between these qubits through three mechanisms. The most prolific of these mechanisms is capacitive coupling, which occur as a result of kinetic terms of the form  $C\dot{\phi}_i\dot{\phi}_j$  coupling the  $\phi_i$  and  $\phi_j$  degrees of freedom. Let us for further reference

define the matrix  $K$  as the symmetric matrix so that the contributions to the Lagrangian from capacitances take the form

$$L_{\text{kin}} = \frac{1}{2} \dot{\phi}^T K \dot{\phi}, \quad (\text{B2})$$

where  $\phi = (\phi_1, \phi_2, \phi_3, \phi_4, \phi_{LR}, \phi_{RR}, \phi_{CM})^T$  is the vector of fluxes. Terms of the form  $C \dot{\phi}_i \dot{\phi}_j$  then constitute off-diagonal contributions to  $K$ , and the strength of the induced interaction between  $\phi_i$  and  $\phi_j$  will be proportional to the  $(i, j)$ -entry in the inverse matrix. It is capacitive couplings that are responsible for the couplings between the left/right qubits and the gate qubits, with the coupling strength given by

$$J_2 = -\frac{1}{4} \left( \frac{E_{J,1} (E_{L,2} + \frac{1}{2} E_{J,2})}{2E_{C,1} E_{C,2}} \right)^{\frac{1}{4}} (2e)^2 (K^{-1})_{(1,3)}, \quad (\text{B3})$$

where  $(K^{-1})_{(i,j)}$  is the  $(i, j)$ -entry in the inverse matrix of  $K$  and  $E_{C,i}, E_{L,i}, E_{J,i}$  are the effective capacitive energies, inductive energies and Josephson energies of the  $i$ 'th qubit. These quantities are related to the circuit parameters as follows:

$$\begin{aligned} E_{C,i} &= \frac{(2e)^2 (K^{-1})_{(i,i)}}{8} \\ E_{J,1} &= E_R \\ E_{L,2} &= \frac{1}{8L} \left( \frac{\Phi_0}{2\pi} \right)^2 + \frac{1}{8L'} \left( \frac{\Phi_0}{2\pi} \right)^2 + \frac{3}{32} (E'_J + E_J + E_q) \\ E_{J,2} &= \frac{E'_J + E_J + 17E_q}{16} \\ E_{J,CM} &= \frac{E_q}{8} \\ E_{L,CM} &= \frac{3E_q}{16} \end{aligned}$$

and comes from writing the single-qubit parts of the Hamiltonian on the form

$$4E_{C,i} \left( \frac{p_i}{2e} \right)^2 + \left( \frac{\Phi_0}{2\pi} \right)^{-2} E_{L,i} \phi_i^2 \quad (\text{B4})$$

$$-E_{J,i} \cos \left( \left( \frac{\Phi_0}{2\pi} \right)^{-1} \phi_i \right), \quad (\text{B5})$$

where  $p_i$  is the conjugate momentum of the  $\phi_i$  degree of freedom and  $\Phi_0$  is the magnetic flux quantum. For brevity, the explicit form of the inverse matrix elements of the inverse of the  $K$  matrix are omitted since these are sizable expressions.

The second effect inducing coupling in the circuit is the presence of the Josephson junctions. These provide terms of the form  $E_J \cos(\phi_i - \phi_j)$ . Since we are in the transmon regime ( $E_J \ll E_C$ ), it is sufficient to expand these cosines to the fourth order in the argument. The result of these terms is therefore, among other things, the

presence of terms of the form  $E_J \phi_2^2 \phi_3^2$ , which later turn into the  $\sigma_z^{(2)} \sigma_z^{(3)}$  coupling. The strength of this coupling is found to be

$$J_z = -\frac{E_{C,2} (E'_J + E_J + 8E_q)}{64 (E_{L,2} + \frac{1}{2} E_{J,2})}. \quad (\text{B6})$$

The  $J_x$ -term contains contributions from both capacitive couplings and Josephson junctions. It also contains contributions from the third and final coupling mechanism: coupling through terms of the form  $\frac{1}{2L} (\phi_i - \phi_j)^2$  coming from the inductors in the central part of the circuit. The interaction strength is given by

$$\begin{aligned} J_x &= \sqrt{\frac{E_{C,2}}{E_{L,2} + \frac{1}{2} E_{J,2}}} \left( \frac{\Phi_0}{2\pi} \right)^2 \left( \frac{1}{4L'} - \frac{1}{4L} \right) \\ &+ \sqrt{\frac{E_{C,2}}{E_{L,2} + \frac{1}{2} E_{J,2}}} \left( \frac{E'_J - E_J}{4} - E_q \right) \\ &+ \frac{1}{4} \sqrt{\frac{E_{L,2} + \frac{1}{2} E_{J,2}}{E_{C,2}}} (2e)^2 (K^{-1})_{(2,3)} \\ &- \frac{E_{C,2} (E'_J - E_J - 10E_q)}{32 (E_{L,2} + \frac{1}{2} E_{J,2})} \\ &+ \frac{E_q}{8} \sqrt{\frac{E_{C,2} E_{C,CM}}{(E_{L,2} + \frac{1}{2} E_{J,2}) (E_{L,CM} + \frac{1}{2} E_{J,CM})}}. \end{aligned} \quad (\text{B7})$$

In addition to the aforementioned couplings, we get the unwanted cross-talk-coupling between the left and right qubit with strength

$$J_4 = \frac{1}{4} \sqrt{\frac{E_{J,1}}{2E_{C,1}}} (2e)^2 (K^{-1})_{1,4}. \quad (\text{B8})$$

Luckily, this problematic coupling can be eliminated by considering the nature of the interaction. By inspecting the circuit, we see that the capacitive interaction yielding  $J_2$  occur through a single resonator, while the  $J_4$  cross-talk-interaction occurs through both of the resonators as well as a capacitance of the central circuit. The effect of each of these additional capacitances is to scale down the strength of the interaction, and so the relative size of  $J_4$  compared to  $J_2$  scales inversely with the capacitances  $C_J$  and  $C_R$ :

$$\left| \frac{J_4}{J_2} \right| \sim \frac{1}{C_J}, \frac{1}{C_R}.$$

By increasing these capacitances, it is therefore possible to scale down the cross-talk to less than 1% of  $J_z$ , which makes the cross-talk sufficiently weak for the transistor to be able to block state transfer with high fidelity (see Section IV).

The frequency of the gate qubits is given by

$$\begin{aligned} \Omega = & -\sqrt{16E_{C,2} \left( E_{L,2} + \frac{1}{2}E_{J,2} \right)} \\ & + \frac{E_{J,2}E_{C,2}}{2 \left( E_{L,2} + \frac{1}{2}E_{J,2} \right)} + \frac{E_{C,2} (E'_J + E_J + 8E_q)}{16 \left( E_{L,2} + \frac{1}{2}E_{J,2} \right)} \\ & + \frac{5E_q}{32} \sqrt{\frac{E_{C,2}E_{C,CM}}{\left( E_{L,2} + \frac{1}{2}E_{J,2} \right) \left( E_{L,CM} + \frac{1}{2}E_{J,CM} \right)}}, \end{aligned} \quad (\text{B9})$$

and the detuning of the left/right qubits from the gate qubits is

$$\Delta = -\sqrt{8E_{C,1}E_{J,1}} + E_{C,1} - \Omega. \quad (\text{B10})$$

This exhausts the list of parameters in Eq. (22).

- 
- [1] H. J. Kimble, “The quantum internet,” *Nature* **453**, 1023–1030 (2008).
- [2] Gershon Kurizki, Patrice Bertet, Yuimaru Kubo, Klaus Mølmer, David Petrosyan, Peter Rabl, and Jörg Schmiedmayer, “Quantum technologies with hybrid systems,” *Proceedings of the National Academy of Sciences* **112**, 3866–3873 (2015).
- [3] I. M. Georgescu, S. Ashhab, and Franco Nori, “Quantum simulation,” *Rev. Mod. Phys.* **86**, 153–185 (2014).
- [4] Helmut Ritsch, Peter Domokos, Ferdinand Brennecke, and Tilman Esslinger, “Cold atoms in cavity-generated dynamical optical potentials,” *Rev. Mod. Phys.* **85**, 553–601 (2013).
- [5] Andreas Reiserer and Gerhard Rempe, “Cavity-based quantum networks with single atoms and optical photons,” *Rev. Mod. Phys.* **87**, 1379–1418 (2015).
- [6] Alexandre Blais, Ren-Shou Huang, Andreas Wallraff, S M Girvin, and R J Schoelkopf, “Cavity quantum electrodynamics for superconducting electrical circuits: An architecture for quantum computation,” *Phys. Rev. A* **69**, 62320 (2004).
- [7] Ze-Liang Xiang, Sahel Ashhab, J. Q. You, and Franco Nori, “Hybrid quantum circuits: Superconducting circuits interacting with other quantum systems,” *Rev. Mod. Phys.* **85**, 623–653 (2013).
- [8] Markus Aspelmeyer, Tobias J. Kippenberg, and Florian Marquardt, “Cavity optomechanics,” *Rev. Mod. Phys.* **86**, 1391–1452 (2014).
- [9] A. W. Glaetzle, K. Ender, D. S. Wild, S. Choi, H. Pichler, M. D. Lukin, and P. Zoller, “Quantum spin lenses in atomic arrays,” *Phys. Rev. X* **7**, 031049 (2017).
- [10] Vlatko Vedral, Adriano Barenco, and Artur Ekert, “Quantum networks for elementary arithmetic operations,” *Physical Review A* **54**, 147 (1996).
- [11] Immanuel Bloch, Jean Dalibard, and Sylvain Nascimbene, “Quantum simulations with ultracold quantum gases,” *Nature Physics* **8**, 267–276 (2012).
- [12] Dimitris I Tsomokos, Sahel Ashhab, and Franco Nori, “Fully connected network of superconducting qubits in a cavity,” *New Journal of Physics* **10**, 113020 (2008).
- [13] Sanjay Gupta and R.K.P. Zia, “Quantum neural networks,” *Journal of Computer and System Sciences* **63**, 355 – 383 (2001).
- [14] P. Rotondo, M. Marcuzzi, J. P. Garrahan, I. Lesanovsky, and M. Müller, “Open quantum generalisation of Hopfield neural networks,” arXiv preprint arXiv:1701.01727 (2017), arXiv:1701.01727.
- [15] Patrick Rebentrost, Thomas R. Bromley, Christian Weedbrook, and Seth Lloyd, “A Quantum Recurrent Neural Network,” arXiv preprint arXiv:1710.03599, 1–14 (2017), arXiv:1710.03599.
- [16] Marcello Benedetti, John Realpe-Gómez, Rupak Biswas, and Alejandro Perdomo-Ortiz, “Quantum-assisted learning of hardware-embedded probabilistic graphical models,” arXiv preprint arXiv:1609.02542 **041052**, 52–54 (2016), arXiv:1609.02542.
- [17] Yudong Cao, Gian Giacomo Guerreschi, and Alán Aspuru-Guzik, “Quantum Neuron: an elementary building block for machine learning on quantum computers,” arXiv preprint arXiv:1711.11240, 1–30 (2017), arXiv:1711.11240.
- [18] JS Otterbach, R Manenti, N Alidoust, A Bestwick, M Block, B Bloom, S Caldwell, N Didier, E Schuyler Fried, S Hong, *et al.*, “Unsupervised machine learning on a hybrid quantum computer,” arXiv preprint arXiv:1712.05771 (2017).
- [19] Leonardo Bianchi, Nicola Pancotti, and Sougato Bose, “Quantum gate learning in qubit networks: Toffoli gate without time-dependent control,” *npj Quantum Information* **2**, 16019 (2016).
- [20] Dave Bacon, Steven T. Flammia, and Gregory M. Crosswhite, “Adiabatic quantum transistors,” *Phys. Rev. X* **3**, 021015 (2013).
- [21] Miroslav Gajdacz, Tomáš Opatrný, and Kunal K. Das, “An atomtronics transistor for quantum gates,” *Physics Letters A* **378**, 1919 – 1924 (2014).
- [22] A. Micheli, A. J. Daley, D. Jaksch, and P. Zoller, “Single atom transistor in a 1d optical lattice,” *Phys. Rev. Lett.* **93**, 140408 (2004).
- [23] J. Y. Vaishnav, Julius Ruseckas, Charles W. Clark, and Gediminas Juzeliūnas, “Spin field effect transistors with ultracold atoms,” *Phys. Rev. Lett.* **101**, 265302 (2008).

- [24] A. Benseny, S. Fernández-Vidal, J. Bagudà, R. Corbalán, A. Picón, L. Roso, G. Birkl, and J. Mompert, “Atomtronics with holes: Coherent transport of an empty site in a triple-well potential,” *Phys. Rev. A* **82**, 013604 (2010).
- [25] Martin Fuechsle, Jill A. Miwa, Suddhasatta Mahapatra, Hoon Ryu, Sunhee Lee, Oliver Warschkow, Lloyd C. L. Hollenberg, Gerhard Klimeck, and Michelle Y. Simmons, “A single-atom transistor,” *Nature Nanotechnology* **7**, 242–246 (2012).
- [26] Supriyo Datta and Biswajit Das, “Electronic analog of the electro-optic modulator,” *Applied Physics Letters* **56**, 665–667 (1990), <https://doi.org/10.1063/1.102730>.
- [27] Michel H Devoret and Christian Glattli, “Single-electron transistors,” *Physics world* **11**, 29 (1998).
- [28] S Gardelis, CG Smith, CHW Barnes, EH Linfield, and DA Ritchie, “Spin-valve effects in a semiconductor field-effect transistor: A spintronic device,” *Physical Review B* **60**, 7764 (1999).
- [29] O. V. Marchukov, A. G. Volosniev, M. Valiente, D. Petrosyan, and N. T. Zinner, “Quantum spin transistor with a Heisenberg spin chain,” *Nature Communications* **7**, 13070 (2016), arXiv:1610.02938.
- [30] Darrick E. Chang, Anders S. Sørensen, Eugene A. Demler, and Mikhail D. Lukin, “A single-photon transistor using nanoscale surface plasmons,” *Nature Physics* **3**, 807 (2007).
- [31] Callum R. Murray and Thomas Pohl, “Coherent photon manipulation in interacting atomic ensembles,” *Phys. Rev. X* **7**, 031007 (2017).
- [32] Wenlan Chen, Kristin M. Beck, Robert Bücker, Michael Gullans, Mikhail D. Lukin, Haruka Tanji-Suzuki, and Vladan Vuletić, “All-optical switch and transistor gated by one stored photon,” *Science* **341**, 768–770 (2013), <http://science.sciencemag.org/content/341/6147/768.full.pdf>.
- [33] J. Hwang, M. Pototschnig, R. Lettow, G. Zumofen, A. Renn, S. Götzinger, and V. Sandoghdar, “A single-molecule optical transistor,” *Nature* **460**, 76–80 (2009).
- [34] Ranojoy Bose, Deepak Sridharan, Hyochul Kim, Glenn S. Solomon, and Edo Waks, “Low-photon-number optical switching with a single quantum dot coupled to a photonic crystal cavity,” *Phys. Rev. Lett.* **108**, 227402 (2012).
- [35] M H Devoret and R J Schoelkopf, “Superconducting Circuits for Quantum Information: An Outlook,” *Science* **339**, 1169–1174 (2013).
- [36] Andrew A. Houck, Hakan E. Türeci, and Jens Koch, “On-chip quantum simulation with superconducting circuits,” *Nature Physics* **8**, 292–299 (2012).
- [37] Yu Chen, C. Neill, P. Roushan, N. Leung, M. Fang, R. Barends, J. Kelly, B. Campbell, Z. Chen, B. Chiaro, A. Dunsworth, E. Jeffrey, A. Megrant, J. Y. Mutus, P. J. J. O’Malley, C. M. Quintana, D. Sank, A. Vainsencher, J. Wenner, T. C. White, Michael R. Geller, A. N. Cleland, and John M. Martinis, “Qubit architecture with high coherence and fast tunable coupling,” *Phys. Rev. Lett.* **113**, 220502 (2014).
- [38] Abhinav Kandala, Antonio Mezzacapo, Kristan Temme, Maika Takita, Markus Brink, Jerry M Chow, and Jay M Gambetta, “Hardware-efficient variational quantum eigensolver for small molecules and quantum magnets,” *Nature* **549**, 242–246 (2017).
- [39] Jens Koch, Terri M Yu, Jay Gambetta, A A Houck, D I Schuster, J Majer, Alexandre Blais, M H Devoret, S M Girvin, and R J Schoelkopf, “Charge-insensitive qubit design derived from the Cooper pair box,” *Phys. Rev. A* **76**, 42319 (2007).
- [40] R. Barends, J. Kelly, A. Megrant, D. Sank, E. Jeffrey, Y. Chen, Y. Yin, B. Chiaro, J. Mutus, C. Neill, P. O’Malley, P. Roushan, J. Wenner, T. C. White, A. N. Cleland, and John M. Martinis, “Coherent josephson qubit suitable for scalable quantum integrated circuits,” *Phys. Rev. Lett.* **111**, 080502 (2013).
- [41] JE Mooij, TP Orlando, L Levitov, Lin Tian, Caspar H Van der Wal, and Seth Lloyd, “Josephson persistent-current qubit,” *Science* **285**, 1036–1039 (1999).
- [42] Caspar H Van der Wal, ACJ Ter Haar, FK Wilhelm, RN Schouten, CJPM Harmans, TP Orlando, Seth Lloyd, and JE Mooij, “Quantum superposition of macroscopic persistent-current states,” *Science* **290**, 773–777 (2000).
- [43] Jérôme Bourassa, Jay M Gambetta, Abdufarrukh A Abdumalikov Jr, Oleg Astafiev, Y Nakamura, and A Blais, “Ultrastrong coupling regime of cavity qed with phase-biased flux qubits,” *Physical Review A* **80**, 032109 (2009).
- [44] Vladimir E Manucharyan, Jens Koch, Leonid I Glazman, and Michel H Devoret, “Fluxonium: Single cooper-pair circuit free of charge offsets,” *Science* **326**, 113–116 (2009).
- [45] John M Martinis, S Nam, J Aumentado, and C Urbina, “Rabi oscillations in a large josephson-junction qubit,” *Physical Review Letters* **89**, 117901 (2002).
- [46] AJ Berkley, H Xu, RC Ramos, MA Gubrud, FW Strauch, PR Johnson, JR Anderson, AJ Dragt, CJ Lobb, and FC Wellstood, “Entangled macroscopic quantum states in two superconducting qubits,” *Science* **300**, 1548–1550 (2003).
- [47] F. Yan, S. Gustavsson, A. Kamal, J. Birenbaum, A. P. Sears, D. Hover, D. Rosenberg, G. Samach, T. J. Gudmundsen, J. L. Yoder, T. P. Orlando, J. Clarke, A. J. Kerman, and W. D. Oliver, “The Flux Qubit Revisited to Enhance Coherence and Reproducibility,” *Nature Communications* **7**, 1–9 (2015), arXiv:1508.06299.
- [48] Sougato Bose, “Quantum communication through an unmodulated spin chain,” *Phys. Rev. Lett.* **91**, 207901 (2003).
- [49] G. M Nikolopoulos, D Petrosyan, and P Lambropoulos, “Coherent electron wavepacket propagation and entanglement in array of coupled quantum dots,” *Europhysics Letters (EPL)* **65**, 297–303 (2004), arXiv:0311041 [quant-ph].
- [50] Luc Vinet and Alexei Zhedanov, “How to construct spin chains with perfect state transfer,” *Physical Review A - Atomic, Molecular, and Optical Physics* **85**, 1–7 (2012), arXiv:arXiv:1110.6474v2.
- [51] M.-H. Yung, “Quantum speed limit for perfect state transfer in one dimension,” *Phys. Rev. A* **74**, 30303 (2006).
- [52] Matthias Christandl, Nilanjana Datta, Artur Ekert, and Andrew J Landahl, “Perfect State Transfer in Quantum Spin Networks,” *Physical Review Letters* **92**, 187902 (2004).
- [53] M Christandl, N Datta, T C Dorlas, A Ekert, A Kay, and A J Landahl, “Perfect transfer of arbitrary states in quantum spin networks,” *Phys. Rev. A* **71**, 32312 (2005).
- [54] A. Metelmann and A. A. Clerk, “Nonreciprocal photon transmission and amplification via reservoir engineering,” *Phys. Rev. X* **5**, 021025 (2015).
- [55] V Balachandran, G Benenti, E Pereira, G Casati, and D Poletti, “Perfect diode in quantum spin chains,” arXiv preprint arXiv:1707.08823 (2017), arXiv:<https://arxiv.org/abs/1707.08823>.
- [56] Anders Sørensen and Klaus Mølmer, “Entanglement and

- quantum computation with ions in thermal motion,” *Phys. Rev. A* **62**, 022311 (2000).
- [57] David C. McKay, Christopher J. Wood, Sarah Sheldon, Jerry M. Chow, and Jay M. Gambetta, “Efficient  $z$  gates for quantum computing,” *Phys. Rev. A* **96**, 022330 (2017).
- [58] Michael A Nielsen and Isaac L Chuang, *Quantum Computation and Quantum Information: 10th Anniversary Edition* (Cambridge University Press, 2010).
- [59] Edward Fredkin and Tommaso Toffoli, “Conservative logic,” *International Journal of Theoretical Physics* **21**, 219–253 (1982).
- [60] Marin Bukov, Luca D’Alessio, and Anatoli Polkovnikov, “Universal high-frequency behavior of periodically driven systems: from dynamical stabilization to floquet engineering,” *Advances in Physics* **64**, 139–226 (2015), <https://doi.org/10.1080/00018732.2015.1055918>.
- [61] J R Johansson, P D Nation, and F Nori, “QuTip: An open-source Python framework for the dynamics of open quantum systems,” *Comp. Phys. Comm.* **183**, 1760–1772 (2012).